Film and Line Tension Effects on the Attachment of Particles to an Interface

III. A Differential Interferometric Method for Determination of the Shapes of Fluid Surfaces

ALEXANDER DUSHKOV NIKOLOV, PETER ATANASSOV KRALCHEVSKY AND IVAN BOYANOV IVANOV[1]

Laboratory of Thermodynamics and Physico-Chemical Hydrodynamics, Faculty of Chemistry, University of Sofia, 1126 Sofia, Bulgaria

Received April 23, 1984; accepted August 15, 1985

A differential interferometric method for experimental determination of the shapes of the bubble cap and the external meniscus is described. The equations of the interference fringes are derived from the equations of the respective surfaces and the conditions for interference. A method for thermodynamic definition of the contact line and experimental measurement of its radius is proposed.

1. INTRODUCTION

In Part I of this series[2] it was shown that the measurement of the film and line tension requires independent determination of the radius of curvature, R_f, of the hat of the fluid particle, attached to the liquid interface (in the case of a bubble the hat is the thin film intervening between the bubble and the bulk gas phase). This could have been done in principle by taking side-view pictures of the system (4) but the precision for the very small bubbles studied by us would have been very low. Perhaps the only technique suitable for our purposes is differential interferometry [see, e.g., Refs. (5–7)]. Although the latter method is widely used for studying solid surfaces, to the best of our knowledge it has been applied to fluid surfaces only by Zorin (8), del Cerro and Jameson (9), and Mingins and Nikolov (10). Unfortunately, neither of the approaches in these works is suitable for the present study. Zorin (8) studied a biconcave meniscus in transmitted light; del Cerro and Jameson (9) and Mingins and Nikolov (10) applied differential interferometry in reflected light to floating lenses. None of these authors has accounted for the gravity deformation of the fluid surfaces whereas for our systems and the precision we require (for calculation of film and line tensions) this effect is of tremendous importance. In addition, the very low intensity of the light reflected by the thin film and the rapid shrinking of the bubble give rise to specific experimental and theoretical problems not encountered by the previous investigators. Hence, in this paper we develop a theoretical approach to the calculation of surface shapes from the observed interference pattern and describe the experimental procedure used.

The paper is organized as follows. In Section 2 we derive the equations allowing the calculation of R_f; Section 3 is devoted to a special, but important, problem—the correct thermodynamic determination of the radius r_c of the three-phase contact line; the experimental procedure and some illustrative results are given in Section 4; the effect of gravity deformation on the interferometric pattern is discussed in somewhat more detail in the Appendix.

[1] Author to whom correspondence should be addressed.

[2] The other papers in this series are quoted hereafter as Part I (1), Part II (2), and Part IV (3).

0021-9797/86 $3.00

2. CALCULATION OF THE HAT (FILM) CURVATURE FROM THE INTERFERENCE PATTERN

The basic principle of differential interferometry consists of splitting the original image into two images. This is achieved by means of two optical wedges in the Mach–Zehnder interferometer (7). We have used only horizontal splitting, when the two images are shifted at a distance d, the so-called "shearing parameter." The light beams coming from the two images interfere, thus creating a rather complicated interference pattern. Some examples are shown in Figs. 1–3. Figure 1 was obtained with a lens (looked at from the top) of methyl caprate of radius 27.2 μm floating over pure water. One observes two distinct kinds of interference fringes—straight lines and circular segments, which we will call "streaks" and "rings," respectively. Note that the number of streaks is equal to the number of rings (if one does not count the central streak) and the two ends of each ring are connected with the ends of a streak over the image of the lens perimeter. The picture was taken with shearing distance $d = 26.42$ μm. Figure 2a shows a smaller lens, whose radius satisfies the condition $r_c < d < 2r_c$ ($r_c = 18.3$ μm, $d = 26.42$ μm). In this case some of the rings are closed and form full circles, whereas others are still connected by streaks. In the limit $2r_c < d$ (Fig. 2b) the two images do not overlap, the streaks are missing, and all rings become full circles. In all these cases, because of the small density difference between the two liquid phases, the water surface is horizontal [if there were any slope it would probably be smaller than 0.1° (11)] and looks uniform in the picture. With a bubble attached to a liquid surface, the deformation of the liquid surface is stronger. This is reflected by the appearance in Fig. 3 of diffuse fringes, which we call "moustaches." The central "dark" streak merges with the central moustache, which far away from the bubble reaches the undeformed surface. The two rings, beginning on the dark streaks, neighboring the central streak (Fig. 3a), are interrupted on the contact line where they give rise to the first two dark moustaches (one on each side). If the surface were deformed more strongly (Fig. 3b), one would observe more

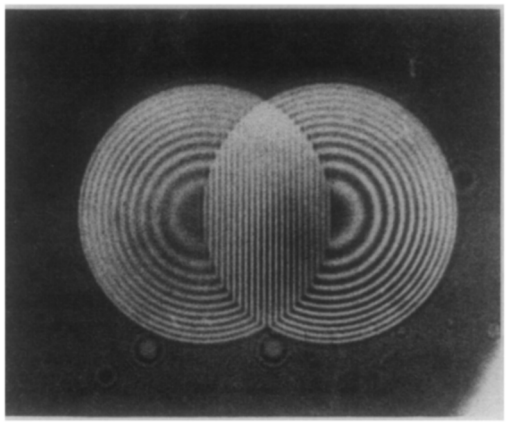

FIG. 1. Differential interference pattern in light reflected from a lens of methyl caprate over water at $d < r_c$ ($r_c = 27.2$ μm and $d = 26.42$ μm).

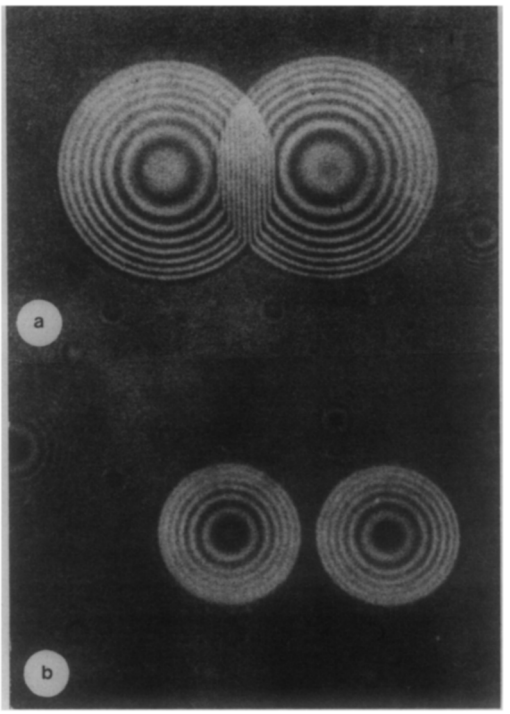

FIG. 2. Differential interference pattern in light reflected from lenses of methyl caprate over water ($d = 26.42$ μm): (a) case $r_c < d < 2r_c$ ($r_c = 18.3$ μm); (*b*) case $2r_c < d$ ($r_c = 12.4$ μm).

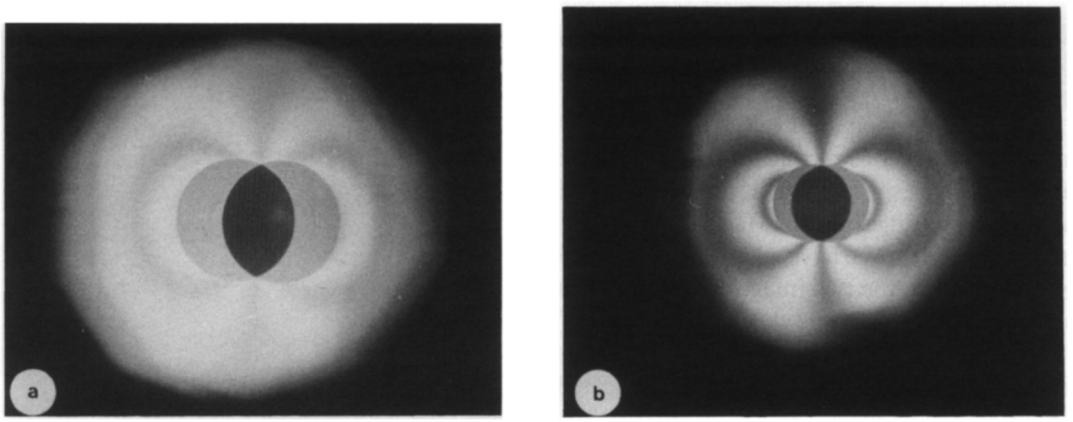

FIG. 3. Differential interference pattern in light reflected from two bubbles, attached to a deformed air/liquid surface. The different number of "moustaches" indicates that the smaller bubble (a) (r_c = 45.4 μm, objective 25×) causes a smaller deformation of the surface than the larger bubble (b) (r_c = 51.7 μm, objective 12.5×).

moustaches and the two ends of each moustache would be connected with the two ends of one (degenerated) ring; this situation is visualized in the lower part of Fig. 4.

We now proceed with the derivation of the equations of the interference fringes and show how to use them to recover from the interference pattern the shapes of the liquid surface and the hat (the upper surface of the lens or the thin film intervening between the bubble and the gas phase). To avoid unnecessary complications part of the derivations are given in the Appendix.

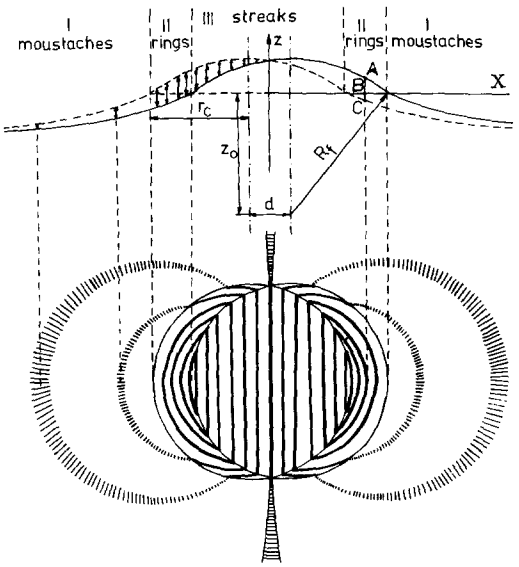

FIG. 4. A sketch of the cross section of the reflecting surfaces shifted at a distance d (upper part) and of the resulting interference pattern (lower part). R_f is the radius and z_0 is the coordinate of the center of the circumference corresponding to the film (the hat); r_c is the radius of the contact line.

The upper part of Fig. 4 is a sketch of the cross section (in the plane $x0z$) of the two images of the reflecting surfaces split at a distance d along the x axis. The plane $x0y$ coincides with the contact line (of radius r_c). R_f is the radius of curvature of the hat (assumed spherical) and

$$z_0 = \sqrt{R_f^2 - r_c^2} \qquad [1]$$

is the coordinate of the center of the respective circumference. The equations of the surfaces are $z = z(x, y)$ and whenever necessary the superscripts "m" and "h" (denoting external meniscus and hat, respectively) and the subscripts "l" and "r" (referring to the left- and right-hand side images) will be used. The lower part of the figure is a sketch of the resulting interference pattern. One clearly discerns three regions corresponding to the interference of light reflected by the two images of the respective surfaces: (i) meniscus–meniscus (moustaches), (ii) meniscus–hat (rings), and

(iii) hat–hat (streaks). In fact, all fringes are loci of points for which the distance between the reflecting surfaces satisfies the requirement

$$|z_l(x, y) - z_r(x, y)| = l_n = n\frac{\lambda}{4};$$

$$n = 0, 1, 2, \ldots, \qquad [2]$$

where λ is the light wavelength and n is the order of interference (n is odd for dark fringes and even for bright fringes). Equation [2] determines the fringe that corresponds to a given n. If the functions $z_l(x, y)$ and $z_r(x, y)$ are continuous, the fringes will be continuous too. In our case, sketched in Fig. 4, this means matching of rings with streaks or moustaches of similar n at the contact lines.

In this paper we assume that the hat is always spherical. For a thin film, whose weight is negligible, this is an excellent approximation [see Part I and (4)]. (For a drop or a lens one can easily account, if necessary, for the gravity deformation of its shape by using the equations derived in Part II.) Hence, the equation of the hat is

$$z^h_{l,r} = \sqrt{R_f^2 - \left(x \pm \frac{d}{2}\right)^2 - y^2} - z_0 \qquad [3]$$

where the upper sign (+) refers to the left-hand side image, and the lower sign (−) to the right-hand side image.

If the deformation of the liquid surface can be neglected, i.e., if $z^m(x, y) \equiv 0$, Eqs. [2] and [3] yield

$$\left(x \pm \frac{d}{2}\right)^2 + y^2 = R_f^2 - (z_0 + l_n)^2. \qquad [4]$$

Therefore in region II one has circles (the rings) that are concentric with the respective images of the contact line,

$$\left(x \pm \frac{d}{2}\right)^2 + y^2 = r_c^2 \qquad [5]$$

and whose radii (cf. Eq. [1])

$$r_n^2 = r_c^2 - l_n^2 - 2l_n\sqrt{R_f^2 - r_c^2} \qquad [6]$$

decrease as n increases. When the liquid surface is deformed, the rings obey Eq. [25]; see the Appendix.

In region III one has

$$|z^h_l(x, y) - z^h_r(x, y)| = l_n \qquad [7]$$

which, along with [3], leads to

$$x^2/a_n^2 + y^2/b_n^2 = 1 \qquad [8]$$

with

$$a_n = b_n/\epsilon_n; \quad b_n = \sqrt{R_f^2 - \epsilon_n^2 l_n^2/4}$$

$$\epsilon_n = (1 + d^2/l_n^2)^{1/2}. \qquad [9]$$

Therefore, the streaks are parts of ellipses and the reason why they look like straight lines is the high eccentricity $\epsilon_n \approx d/l_n \gg 1$ (see below). By making use of the exact equations of the interference fringes (Eqs. [8], [14], and [25]) one can describe theoretically the transition of streaks to rings and then to moustaches, observed experimentally as described above (see the Appendix).

The hat curvature is most conveniently calculated from the coordinates, x_n, of the intersection of the streaks or rings (more precisely, of the lines with maximum intensity) with the x axis. The result for the **streaks** can be derived by setting, in [8], $y = 0$. Thus, using also Eqs. [9], we obtain

$$R_f = \epsilon_n\sqrt{x_n^2 + l_n^2/4}; \qquad [10]$$

one observes that $x_n = a_n$.

The function $R_f(x_n)$ for the **rings** is derived from the following simple geometric considerations. From Fig. 4 one has $AC = AB + BC$, where $AC = l_n$, $AB = z^h_r(x_n, 0)$ and $BC = Q(x_n + d/2)$. Here (cf. Eq. [72] of Part II)

$$Q(x) = r_c\left\{\left[\operatorname{arc\,cosh}\left(\frac{x}{r_c \sin\psi_c}\right) - \operatorname{arc\,cosh}\left(\frac{1}{\sin\psi_c}\right)\right]\sin\psi_c - (qr_c)^2\left[F\left(\frac{x}{r_c\sin\psi_c}\right) - F\left(\frac{1}{\sin\psi_c}\right)\right]\right\}, \qquad [11]$$

where $q = (\Delta\rho g/\sigma)^{1/2}$ ($\Delta\rho$ is the density difference between the liquid and gas phases, σ is

the liquid/gas surface tension, g is the gravity acceleration, and ψ_c is the slope angle of the external meniscus at the contact line) and the function F is defined by Eq. [69] in Part II. By introducing the notation

$$D_n \equiv l_n - Q\left(x_n + \frac{d}{2}\right) = z_\tau^h(x_n, 0) \quad [12]$$

and making use of [3] and [1] one obtains

$$R_f^2 = r_c^2 + \left[\frac{r_c^2 - D_n^2 - (x_n - d/2)^2}{2D_n}\right]^2. \quad [13]$$

The hat does not contribute to the formation of the moustaches. Therefore, they can be used only for the calculation of r_c. The respective equation can be derived from the relationship

$$l_n = Q\left(x_n - \frac{d}{2}\right) - Q\left(x_n + \frac{d}{2}\right). \quad [14]$$

However, this equation is of little avail because of the diffusivity of the moustaches. Some other characteristic points of the moustaches might prove to be more useful than x_n, but we will not dwell on this point.

3. ON THE THERMODYNAMIC DEFINITION OF THE RADIUS OF THE CONTACT LINE

As already pointed out in Part I in close vicinity of the contact line the surface tensions no longer have their macroscopic values. The shapes of the interfaces also deviate from what they would be if the surface tensions were constant. It is therefore paramount to have a correctly defined radius of the contact line, r_c, in order to obtain reliable values for the thermodynamic characteristics of the system.

With sufficiently thin films the reflecting surfaces undergo an abrupt change of slope at the contact line, so that the image of the contact line is sharp and one can measure its radius with high precision. However, when the film is thicker, the slopes of the interfaces at the contact line may change so little that the location of the contact line becomes uncertain. Moreover, the transition region, where the surface tensions deviate from their macroscopic values, can then, in principle, be large enough to include some parts of the surfaces that give rise to the interference fringes. As pointed out in Part I, under these conditions the only correct way of defining the contact line is to solve the Laplace equation for the three surfaces (external meniscus, hat, and lower surface of the bubble) and to extrapolate the solutions at constant (macroscopic) surface tensions until they intersect.

For the system considered here this problem can be resolved by making use of Eqs. [10] and [13]. If all streaks yield the same value of R_f, the transition region does not affect the fringes. (Incidentally, if it did, there would be a smooth transition from streaks to rings instead of a break.) If the same value of R_f is obtained from Eq. [13] (which contains (r_c), this is a guarantee that r_c has been correctly measured. On the contrary, if either of these conditions is not met, one can proceed in the following way: one calculates R_f from [10] for these streaks that yield a constant value of R_f. It is then substituted in [13] and one calculates r_c from those rings that yield the same value for r_c. Although simple and in principle impeccable, this procedure is connected with considerable computational difficulties, because calculation of ψ_c also requires knowledge of r_c. Hence, we propose below an iterative procedure (for details and notations see Part II).

(i) One measures experimentally an approximate value of r_c (denoted by r_c^0) which will serve as a zeroth approximation.

(ii) From the experimentally measured radius of the equator of the bubble, R, and Eq. [15] of Part II

$$b = R\left[1 - \frac{\beta}{6} + \frac{\beta^2}{6}\left(\ln 2 - \frac{1}{6}\right)\right]^{-1}, \quad \beta = (qb)^2 \quad [15]$$

one determines b (the radius of curvature at the bottom of the bubble) by iterations, using R as a zeroth approximation for b.

(iii) From Eq. [13] of Part II

$$\sin \varphi_c = r_c/b - \beta u_1(\varphi_c) - \beta^2 u_2(\varphi_c) \quad [16]$$

one calculates φ_c, using $\varphi_c^{(0)} = \arcsin(r_c/b)$ as a zeroth approximation.

(iv) From Eq. [13] of Part IV

$$\sin\psi_c = \frac{r_c}{b}\left[1 + \frac{\beta}{2b}(z_c - h_c)\right] - \sin\varphi_c,$$

where $z_c(\varphi_c)$ and $h_c(\psi_c)$ are defined by Eqs. [14] and [71] of Part II, one calculates ψ_c by iterations using $\psi_c = 0$ as a zeroth approximation.

(v) From [11] and [12] one calculates D_n.

(vi) From the equation

$$r_c = \left[\left(x_n - \frac{d}{2}\right)^2 + 2D_n \times \sqrt{R_f^2 - \left(x_n - \frac{d}{2}\right)^2} - D_n^2\right]^{1/2} \quad [17]$$

(which follows from [1], [3], and [12]) one calculates the first iteration of r_c, using the constant value of R_f determined from the streaks. Then, one starts over with step iii. Note that the procedure makes use of equations for the three interfaces, which intersect at the contact line.

To demonstrate the feasibility and the precision of this procedure we have applied it to a photograph of one bubble with $R = 118.6$ μm ($b = 118.7$ μm) and $R_f = 240.8$ μm (determined from the streaks). The results are shown in Table I for three rings. For each ring three zeroth approximations, r_c^0, have been used (25, 30, and 35 μm) and all of them lead to the same results, shown in the last column. The calculated average value $r_c = 30.0 \pm 0.1$ μm is in excellent agreement with the directly measured (from the photograph) value, 30.04 μm.

TABLE I

Order of interference n	Ring coordinate x_n (μm)	Calculated r_c (μm)
4	32.1	30.0
6	29.2	30.0
8	25.5	29.9

4. EXPERIMENTAL PROCEDURE AND RESULTS

A detailed description of the experimental procedure and the materials used is given in Part IV. We describe here only the interferometric techniques and the procedure used to determine the radius of curvature of the hat, R_f. The experiments were carried out with a differential microscope (Epival Interphako) using an eyepiece (×16) and objective (×25). The light source was a high-pressure mercury lamp (HBO-50, 50 W) combined with an interferometric filter with $\lambda = 0.546$ μm. When a single slit was being used the image lacked contrast. That is why we used the multiple slit 48. The value of the shearing parameter used, $d = 12.08 \pm 0.02$ μm (in some experiments $d = 24.16$ μm), was determined as described in the manual for the microscope (10). The focal depth of the objective used was found to be ± 2.5 μm. The aperture correction was determined by performing measurements of the radii of curvature of model systems (Nikolov, Kralchevsky, Dimitrov, to be published) and since it turned out to be random and smaller than 1.5%, it was assumed to be zero.

All examples of measurements of R_f given in the present paper were obtained with 0.05% solutions of sodium dodecyl sulfate (Fisher Scientific) containing 0.25 kmole/m^3 NaCl. We must point out that the films formed by these solutions are so thin that they are almost absolutely transparent; they look black in reflected light. As low as the intensity of the light reflected by these films might be, it is sufficient, as our experiments proved, to produce differential interference fringes. However, we must warn the potential user of this method that we were able to obtain sufficiently good interference patterns only when we took extreme care to avoid all possible perturbations (especially vibrations) and strictly observed the experimental conditions as formulated in the beginning of this section; for example, the replacement of the multiple slit by a single slit would considerably worsen the quality of the picture.

Due to the diffusion of the gas across the film, the gas bubble dimensions steadily de-

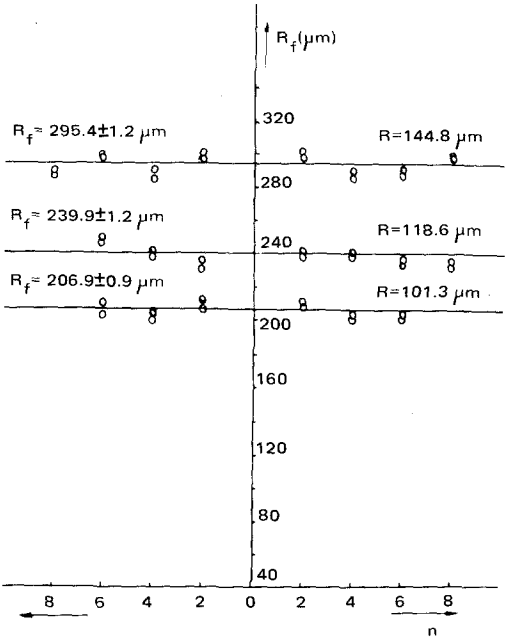

FIG. 5. The results for the radius of curvature of the film R_f (calculated from streaks) as a function of the interference order n for three bubbles, whose equatorial radii R are also shown on the figure. The lines correspond to the average values of R_f, calculated by means of the minimization procedure, as explained in the text.

crease with time. Down to bubble radii $R \approx 80$ μm it was possible to take pictures (with exposure times of 8–9 s) and to measure from the photographs the distance between the fringes with sufficient precision. With smaller bubble radii the shrinking of the bubble was so rapid that only visual observations were possible (see below).

The experimental results and their use in calculation of the full set of system parameters are described in Part IV. In this paper we give only a few illustrative examples to show how the film curvature is calculated from the experimental data and to emphasize the need to correctly account for the gravity effects in order to obtain reliable results.

The R_f values calculated from the streaks and Eq. [10] are extremely sensitive to the coordinates x_n. While it is relatively easy to find the **distance** between two symmetric streaks, it is much more difficult to locate the axis of symmetry of the picture, i.e., to find the zero of the axis $0x$ (see Fig. 4). The best procedure is to measure the coordinates x_n of the fringes with respect to an arbitrarily chosen origin of the coordinate axis and to construct the function

$$\Phi(a') = \sum_n [R_f(x'_{ln} - a') - R_f(x'_{rn} - a')]^2 \quad [18]$$

where x'_{ln} and x'_{rn} are the coordinates of each pair of symmetric streaks and $R_f(x'_{ln} - a')$ and $R_f(x'_{rn} - a')$ are calculated from Eq. [10]; the summation is carried out over all pairs of symmetric streaks. The value $\bar{a}$ of a', which minimizes the function $\Phi(a')$, is the most probable value of the coordinate of the center, and $x_n = x'_n - \bar{a}$ are the coordinates of the streaks with respect to this center.

Figure 5 shows the results for R_f calculated in this way from three photographs (R_f = 295.4, 239.9, and 227.7 μm). The coordinate of each streak was measured twice from the photographs and the two points for a given n correspond to the two values of R_f calculated from these two measurements. The standard deviation is shown in the figure.

An important check on the precision of the experimental procedure is the comparison of the R_f values calculated independently from streaks (Eq. [10]) and rings (Eq. [13]) for the same photograph. This was possible only when the elevation of the hat over the contact line was small enough so that both the streaks and the rings appeared distinctly on the photograph. Two examples are given in Table II; the differences are within the range of the standard deviation.

TABLE II

R_f Calculated Independently from Streaks (Eq. [10]) and Rings (Eq. [13])

r_c (μm)	R (μm)	R_f (μm)	
		Streaks	Rings
30.0	118.6	240.8 ± 3.8	242.8
27.6	110.9	224.7 ± 5.3	225.6

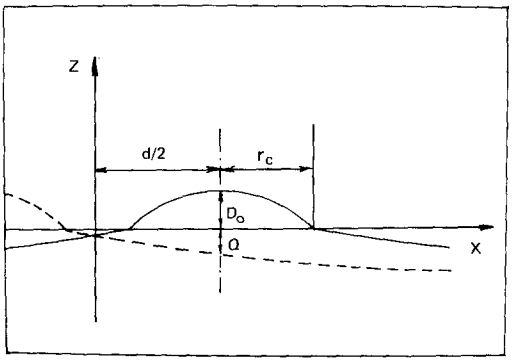

FIG. 6. A scheme of the reflecting surfaces in the case of complete splitting (shearing distance $d > 2r_c$).

Visual determination of R_f was performed with complete splitting (see Fig. 2b), i.e., with $r_c < d/2$ (d was increased to 24.16 μm in this case in order to avoid a gap between photographic and visual measurements). The essence of the method is to record r_c at the moment when the top ring shrinks to a point. From Fig. 6 it follows that at this moment

$$D_0 + Q(d) = l_n \qquad [19]$$

(Q is again calculated from Eq. [11]). Then Eq. [13] written for $x_n = d/2$ leads to

$$R_f = \frac{r_c^2 + D_0^2}{2D_0} . \qquad [20]$$

The error involved in this procedure can be estimated by means of the following semiquantitative considerations. Let us assume that the width of a fringe (along the axis $0z$) is $\lambda/4$: (i) if the top ring is dark the bright spot within it will disappear when the location of the ring (more precisely, of its darkest part) is at a distance $\Delta l \approx \lambda/8$ from the pole of the hat; (ii) the pole will become darker than its environment when $\Delta l < \lambda/16$; (iii) the intensity at the pole will be maximum at $\Delta l = 0$ (this corresponds to the condition [19]); and (iv) the dark spot will completely disappear when the ring is at a distance $\lambda/8$ above the pole. The radius of the dark spot in any of these cases is of the order of $\sqrt{2R_f\Delta l}$. Simple calculations show that an error Δl in l_n leads to an error $\Delta r_c \approx (R_f/r_c)\Delta l$ and, according to [20],

$$\Delta R_f \approx (R_f/l_n)\Delta l. \qquad [21]$$

Experimentally the moment t_1 of disappearance of the spot inside the ring (situation i above, $|\Delta l| = \lambda/8$) is established by changing several times the brightness of the top ring from dark to bright and vice versa (by means of the micrometric screw inside the Max–Zehnder interferometer). The moment t_2 of complete disappearance of the dark spot itself (situation iv above, $|\Delta l| = \lambda/8$) is established in the same way. The average time, $t = (t_1 + t_2)/2$, will approximately correspond to situation iii, i.e., to $\Delta l = 0$. The respective value of r_c is taken from the experimental curve $r_c = r_c(t)$ (see Part IV). The same procedure was followed when the top ring was bright. By counting the number k of the rings of the same brightness as the top spot one calculates l_n: if the liquid surface is visually planar (no moustaches) and has the same brightness as the top spot, $l_n = k(\lambda/2)$; in the opposite case, $l_n = k(\lambda/2) - \lambda/4$. If there are also moustaches, they must be accounted for when calculating l_n. The error is within the range $0 < \Delta l < \lambda/16$. For our visual measurements $l_n \geq 2\lambda$ and $R_f \leq 100$ μm (see Table IV) so that from Eq. [21] $\Delta R_f \leq 3$ μm.

In conclusion we quote a few data demonstrating the importance of the gravity correction Q for the correct calculation of R_f. Table III refers to a photograph of a relatively small bubble: $r_c = 30.0$ μm, $R = 118.6$ μm, and $\psi_c = 0.636°$. Each row corresponds to a

TABLE III

Values of R_f for a Photograph Calculated from Rings (Eq. [13]) with and without Gravity Correction Q

x_n (μm)	l_n (μm)	Q (μm)	R_f (μm) Eq. [13]	R_f (μm) With $Q = 0$
32.06	0.546	0.079	242.8	208.0
29.16	0.819	0.053	241.5	226.1
25.54	1.092	0.017	244.1	240.4

TABLE IV

Values of R_f from Visual Measurements for Two Bubbles with and without Gravity Correction Q

r_c (μm)	R (μm)	ψ_c (°)	l_n (μm)	Q (μm)	R_f (μm)	
					Eq. [20]	With $Q = 0$
15.8	70.5	0.25	0.9555	0.0298	135.6	131.3
13.4	60.7	0.19	0.8190	0.0266	113.6	109.9

ring. The last column contains the R_f values that one would have obtained if the gravity correction were neglected. One clearly sees that although Q is more than one order of magnitude smaller than l_n it strongly affects the values of R_f. Note that the gravity correction varies with the number of the ring; the latter is also evident from Eq. [11].

Even with very little bubbles, when the liquid surface seems uniform Q should not be disregarded. This is demonstrated in Table IV containing data from visual measurements ($d = 24.16$ μm) for two bubbles.

APPENDIX

RINGS, STREAKS, MOUSTACHES, AND THEIR CONNECTION

Equations of the rings (in the presence of gravity) and the moustaches are derived again from the general condition [2]. The generatrix of the external meniscus is given by Eq. [74] of Part II. The two images of the external meniscus have cylindrical symmetry around the axes passing through $x = \pm d/2$ and parallel to $0z$. Hence, we introduce the cylindrical coordinates (not to be confused with r_c)

$$r_{l,r} = \left[\left(x \pm \frac{d}{2}\right)^2 + y^2\right]^{1/2} \qquad [22]$$

where the subscripts "l" and "r" again denote left- and right-hand side images, respectively. Then the distance BC (see Fig. 4) of the external meniscus from the plane $z = 0$ will again be given by [11] if the argument x is replaced by r_l or r_r. In this way for the equations of the right-hand side rings ($x > 0$) one has (cf. the derivation of [13])

$$l_n = Q(r_l) + z_r^h(x, y) \qquad [23]$$

and similarly for $x < 0$. Defining

$$D_n(r_l) = l_n - Q(r_l) \qquad [24]$$

and using [1] and [3] we thus obtain

$$(x - d/2)^2 + y^2 = r_c^2 - 2D_n\sqrt{R_f^2 - r_c^2} - D_n^2. \qquad [25]$$

If there were no gravity deformation, $Q(r) \equiv 0$, $D_n \equiv l_n$, and the right-hand side of [25] would coincide with [6]; i.e., the rings would have been perfect concentric circles. In the presence of gravity the rings deviate from this shape. The equation of the moustaches (for $x > 0$) is

$$l_n = Q(r_r) - Q(r_l). \qquad [26]$$

The coordinates x_s and y_s of the intersection of a streak with the left-hand side image of the contact line are obtained by solving together Eqs. [8] and [5] (with upper sign). The result is

$$x_s = \frac{l_n}{d}\left(\sqrt{R_f - r_c^2} + \frac{l_n}{2}\right);$$

$$y_s = \pm\sqrt{r_c^2 - \left(x_s + \frac{d}{2}\right)^2}. \qquad [27]$$

It is easily shown that the coordinates of the intersection points of a circular ring lying at $x > 0$ (lower sign in [4]) with the left-hand side image of the contact line are again given by [27]. Indeed, over the left-hand side image of the contact line $r_l = r_c$ and $Q(r_l) = 0$ (see Eq. [11]), $D_n(r_c) = l_n$, so that [25] transforms

into [4] and the intersection points remain the same. Therefore, whatever the deformation of the surface, a ring always starts over the intersection point of a streak with the contact line.

ACKNOWLEDGMENTS

The authors are indebted to Professor M. Françon and Professor R. Dupeyrat, who read the manuscript and made valuable comments.

REFERENCES

1. Ivanov, I. B., Kralchevsky, P. A., and Nikolov, A. D., *J. Colloid Interface Sci.* **112,** 97 (1986).
2. Kralchevksy, P. A., Ivanov, I. B., and Nikolov, A. D., *J. Colloid Interface Sci.* **112,** 108 (1986).
3. Kralchevsky, P. A., Nikolov, A. D., and Ivanov, I. B., *J. Colloid Interface Sci.* **112,** 132 (1986).
4. Princen, H. M., and Mason, S. G., *J. Colloid Sci.* **20,** 353 (1965).
5. Françon, M., "Progress in Microscopy," p. 207. Pergamon Press, London, 1961.
6. Françon, M., and Mallick, S., "Polarization Interferometers," p. 101. Wiley-Interscience, New York, 1971.
7. Beyer, H., "Theorie und Praxis Der Interferenzmikroskopie." Akademische Verlagsgeselschaft, Leipzig, 1974.
8. Zorin, Z. M., *Kolloidn. Zh.* **39,** 1158 (1977).
9. del Cerro, M. C. G., and Jameson, G. J., *in* "Wetting, Spreading and Adhesion" (J. F. Padday, Ed.), p. 61. Academic Press, New York, 1978.
10. Mingins, J., and Nikolov, A. D., *Ann. Univ. Sofia (Fac. Chim.)* **75** (1980/1981), [in Bulgarian] **75,** 3 (1981).
11. Hoffman, R., and Gross, L., *J. Microsc.* **91,** 149 (1970).